Synthesis and Characterization of Film-Forming Colloidal Nanocomposite Particles Prepared via Surfactant-Free Aqueous Emulsion Copolymerization

Andreas Schmid, Peter Scherl, and Steven P. Armes*

Department of Chemistry, Dainton Building, The University of Sheffield, Brook Hill, Sheffield S3 7HF, United Kingdom

Carlos A. P. Leite and Fernando Galembeck

Universidade Estadual de Campinas, Instituto de Química, P.O.Box 6154, Campinas SP, São Paulo 13083-862, Brazil

Received March 3, 2009; Revised Manuscript Received March 30, 2009

ABSTRACT: The efficient synthesis of film-forming colloidal nanocomposite particles is described. A 50:50 mass ratio of styrene and *n*-butyl acrylate is statistically copolymerized using a cationic azo initiator at 60 °C under aqueous emulsion polymerization conditions in the presence of a commercially available glycerol-functionalized ultrafine silica sol. This new formulation leads to the production of copolymer/silica particles with relatively narrow size distributions and a well-defined "core−shell" morphology. These nanocomposite particles contain up to 43% silica by mass, and the silica aggregation efficiency can exceed 95%, so very few nonaggregated silica nanoparticles remain in solution after the in situ copolymerization is conducted. Upon drying these dispersions, highly transparent free-standing nanocomposite films are obtained. Control experiments confirm the importance of using the cationic azo initiator in combination with the glycerol-functionalized silica sol. Moreover, it is also shown that simple admixtures of a film-forming copolymer latex with the glycerol-functionalized silica sol give much more opaque nanocomposite films, while the deliberate addition of excess silica sol prior to nanocomposite film formation leads to extensive film cracking. Thus this in situ copolymerization route appears to offer a decisive advantage for nanocomposite coatings applications.

Introduction

There is increasing interest in the synthesis of colloidal nanocomposite particles, particularly those comprising vinyl polymers and silica. An early summary of this field was published in 2002,[1] but three new reviews have recently appeared.[2−4] Such inorganic/organic hybrid particles have numerous applications, ranging from next-generation exterior façade paints[5] to pH-responsive Pickering emulsifiers[6,7] to model projectiles for mimicking the behavior of cosmic dust.[8] Our group pioneered the (co)polymerization of vinyl monomers in the presence of ultrafine silica sols as a facile synthetic route to colloidal nanocomposite particles.[9−13] In the specific context of film-forming nanocomposite particles, Armes and coworkers[13] reported the surfactant-free emulsion copolymerization of 4-vinylpyridine with *n*-butyl acrylate in the presence of a 20 nm aqueous silica sol using an anionic persulfate initiator. After careful purification to remove the excess nonaggregated silica sol, film-forming colloidal vinyl polymer-silica nanocomposites were obtained with mean diameters ranging from 139 to 305 nm and silica contents of 20 to 56 wt %. Highly transparent films could be readily obtained by solution casting at room temperature. For example, a 150 μm film showed a transparency of more than 85% at wavelengths greater than 400 nm. X-ray photoelectron spectroscopy (XPS) measurements revealed morphological changes during film formation. The original nanocomposite particles typically had silica-rich surfaces, whereas the surface of the final nanocomposite films was predominately copolymer-rich. Tiarks et al.[14] copolymerized 4-vinylpyridine with *n*-butyl acrylate in the presence of a silica sol under miniemulsion conditions; this elegant approach led to the formation of nanocomposite particles with very high silica aggregation efficiencies. Miniemulsion polymerization was also studied by Wu and coworkers.[15] Silica particles ranging from 45 to 250 nm diameter were surface-functionalized using 3-methacryloyloxypropyltrimethoxysilane (MPS) and used for the miniemulsion copolymerization of a styrene/*n*-butyl acrylate comonomer mixture. This resulted in various particle morphologies ranging from core−shell to raspberry morphologies, depending on the size of the silica particles. Similarly, Qi et al.[16] prepared poly(methyl methacrylate-*stat*-*n*-butyl acrylate)/silica nanocomposite particles via miniemulsion polymerization using MPS-functionalized silica particles. Percy et al. reported the synthesis of film-forming nanocomposites by emulsion polymerization of either methyl acrylate or *n*-butyl acrylate using commercial alcoholic silica sols;[11] films of approximately 150 μm thickness exhibited transparencies of over 92% between 400 and 800 nm.

In summary, previous film-forming nanocomposite syntheses have always required the use of either miniemulsion polymerization,[14−16] auxiliary comonomers,[13] alcoholic silica sols,[11,17] or in situ surface functionalization of the silica sol.[15,16] Each of these approaches has obvious disadvantages in terms of convenience, cost, or the undesirable introduction of volatile organic compounds. In a recent communication, we reported an improved protocol for the synthesis of film-forming poly(styrene-*stat*-*n*-butyl acrylate)/silica nanocomposite particles using a commercially available glycerol-modified Bindzil CC silica sol.[18] A follow-up paper based on a polystyrene/silica formulation has just been published.[19] This non-film-forming model system offers important advantages for several characterization techniques, in particular, electron microscopy. In the present work, we describe our full set of data obtained with more commercially relevant film-forming poly(styrene-*stat*-*n*-

* To whom correspondence should be addressed. E-mail: s.p.armes@sheffield.ac.uk.

10.1021/ma900465k CCC: $40.75
Published on Web 04/23/2009

butyl acrylate)/silica nanocomposite particles, along with several important control experiments that demonstrate (i) the "added value" of the in situ (co)polymerization approach to colloidal nanocomposite particles and (ii) the deleterious effect of excess silica sol on nanocomposite film transparency.

Experimental Section

Materials. Styrene and *n*-butyl acrylate were purchased from Aldrich, passed in turn through a basic alumina column to remove inhibitor and then stored at −20 °C prior to use. 2,2′-Azobis(isobutyramidine) dihydrochloride (AIBA) was used as received from Aldrich. The commercial glycerol-functionalized silica particles (Bindzil CC40; nominal 12 nm diameter aqueous silica sol at 40 wt % according to the manufacturer) was obtained from Eka Chemicals (Bohus, Sweden) and was also used as received. Our in-house TEM study of this silica sol suggested an actual mean particle diameter of 19 nm. Deionized water (pH 6) was used in all experiments.

Nanocomposite Particle Synthesis. A typical nanocomposite synthesis was carried out as follows. The appropriate amount of the aqueous silica sol (8.11 g aqueous dispersion, which is equivalent to 3.0 g dry silica) was diluted with water (35.9 g) and placed in a round-bottomed flask containing a magnetic stir bar, followed by the addition of styrene (2.5 g) and *n*-butyl acrylate (2.5 g). This emulsion was degassed by five evacuation/nitrogen purge cycles and subsequently heated to 60 °C in an oil bath. The AIBA initiator (50.0 mg; 1.0 wt % based on comonomer) was dissolved in 4.0 g of degassed water and added to give a total mass of water of 45 g. Each copolymerization was allowed to proceed for 24 h. The resulting milky-white colloidal dispersions were purified, if required, by repeated centrifugation−redispersion cycles (5000−7000 rpm for 30 min.) using a refrigerated centrifuge (5 °C), with each successive supernatant being carefully decanted and replaced with water. Redispersion was achieved by agitation on a roller mixer for a few hours (N.B. ultrasonic treatment was avoided because it is usually accompanied by a rise in temperature, which can lead to film formation instead of redispersion). This purification protocol was repeated for up to five cycles for selected samples until TEM studies confirmed that all excess silica sol had been removed.

A cationic copolymer latex was prepared for control experiments by emulsion copolymerization of 2.5 g styrene and 2.5 g *n*-butyl acrylate in 45 g water containing a nonionic surfactant (Triton X100, 60 mg, Aldrich) using AIBA initiator (50.0 mg) at 60 °C for 24 h. DLS studies revealed a mean intensity-average particle diameter of 443 nm and a polydispersity index of 0.04. An anionic copolymer latex was also prepared by emulsion copolymerization of 2.5 g styrene and 2.5 g *n*-butyl acrylate in 45 g water containing anionic sodium dodecyl sulfate surfactant (15 mg, Aldrich) using ammonium persulfate initiator (50 mg, Aldrich) at 60 °C for 24 h. Dynamic light scattering measurements revealed a mean intensity-average particle diameter of 240 nm and a polydispersity index of 0.02. Excess surfactant was removed by dialysis in deionized water in both cases.

Characterization of Nanocomposite Particles and Films. *Particle Size Analyses.* DLS (Malvern Zetasizer NanoZS) was used to obtain intensity-average particle diameters. Disk centrifuge photosedimentometry (DCP, Brookhaven Instruments) was used to obtain the weight-average particle size distributions of the purified nanocomposite particles. Run times were between 15 and 30 min with typical centrifugation rates of 6000 to 8000 rpm. Solid-state nanocomposite densities were measured by helium pycnometry (Micromeritics AccuPyc 1330 instrument).

Thermogravimetric analyses (TGA) were conducted using a Perkin-Elmer Pyris 1 TGA instrument. Samples were predried in an oven at 70 °C for 12 h and then heated in air to 800 °C at a heating rate of 10 °C/min. The observed mass loss was attributed to complete pyrolysis of the copolymer component, with the remaining incombustible residues being assumed to be pure silica (SiO_2).

Transmission electron microscopy samples were prepared by drying a drop of a dilute aqueous dispersion on a carbon-coated copper grid. Analysis was conducted using a Phillips CM100 instrument operating at 100 kV.

Particle growth and comonomer conversion curves were determined by periodic sampling of the copolymerizing solution. Quenching was achieved by exposure to air and cooling to ambient temperature. Solids contents were determined gravimetrically with an Ohaus M45 moisture analyzer at a drying temperature of 150 °C, and DLS particle diameters were measured after dilution with water.

Aqueous electrophoresis measurements were conducted using a Malvern Zetasizer NanoZS instrument. Measurements were carried out in the presence of 1.0 mM KCl as background salt, and the solution pH was adjusted by the addition of HCl or KOH. The solution pH was adjusted to around 11 and then titrated to pH 1.5.

Film transparencies were assessed by visible absorption spectroscopy using a Perkin-Elmer Lambda 25 spectrometer. Spectra were recorded from 190 to 1100 nm at a scan speed of 960 nm/min.

XPS studies were conducted using a Kratos Axis Ultra 'DLD' X-ray photoelectron spectrometer equipped with a monochromatic Al Kα X-ray source ($h\nu = 1486.6$ eV) operating at a base pressure in the range of 10^{-8} to 10^{-10} mbar.

Electron Spectroscopy Imaging by Transmission Electron Microscopy (ESI/TEM). The nanomorphology and the spatial elemental distribution within the copolymer−silica nanocomposite particles were assessed by ESI/TEM using a Carl Zeiss CEM 902 transmission electron microscope equipped with a Castaing−Henry−Ottensmeyer filter spectrometer within the column. The nanocomposite particle dispersions were dried at room temperature under air, and the resulting solids were embedded in a soft epoxy resin that was cured for 24 h at room temperature, followed by 24 h in an oven at 60 °C. The resin blocks were trimmed and cut in an EM FC6 Leica ultramicrotome using a Diatome diamond knife. Ultrathin sections of approximately 40 nm thickness were collected over copper grids for ESI/TEM analysis. ESI images were acquired by the three-windows method using electrons with element-specific threshold energies (101 eV for silicon and 284 eV for carbon) supported by iTEM imaging platform (Olympus) and recorded using a slow-scan CCD camera (Proscan).[20]

Silica incorporation efficiencies were determined by two separate methods. The first method involved determining the monomer conversion gravimetrically after each polymerization and also the mean silica content of purified dried nanocomposite samples obtained by thermogravimetric analysis. The second method involved centrifugation of the reaction solution at 13 000 rpm for 10 min, followed by gravimetric analysis of the solids content of the supernatant. This approach gives the free excess silica sol directly, provided that the nanocomposite particles are fully sedimented and all of the excess silica sol remains in the supernatant phase. If some of the silica sol is also inadvertently sedimented under these conditions, then the calculated silica aggregation efficiency will represent an upper limit value. Although such sedimentation of excess silica sol cannot be ruled out, a comparative test in which the diluted silica sol was subjected to centrifugation under identical conditions suggested that only minimal sedimentation occurred. The estimated error in the final silica aggregation efficiencies is ±2%.

Results and Discussion

Film-forming nanocomposite particles were readily prepared by emulsion copolymerization of styrene and *n*-butyl acrylate using a cationic azo initiator in the presence of a commercial aqueous glycerol-functionalized silica sol. A schematic representation of this synthesis protocol is shown in Figure 1. The effect of varying the silica sol concentration and comonomer mass ratio in such syntheses is summarized in Table 1.

Influence of Silica Sol Mass. Our very recent study of high T_g polystyrene/silica nanocomposite particles[19] using essentially the same synthesis protocol confirmed that the initial silica sol concentration had a pronounced effect on nanocomposite particle

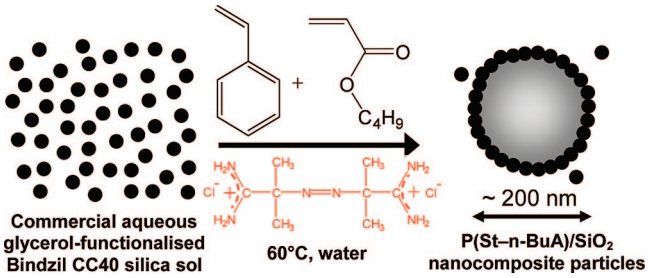

Figure 1. Schematic representation of the synthesis of nanocomposite particles by emulsion copolymerization of styrene with *n*-butyl acrylate using a cationic azo initiator (AIBA) in the presence of a commercial ultrafine glycerol-modified aqueous silica sol (Bindzil CC40) as the sole stabilizing agent.

properties: higher silica sol concentrations generally led to a reduction in mean particle diameter but also to lower silica sol incorporation efficiencies. The present work is focused on low T_g film-forming copolymer compositions: the initial silica sol concentration was varied between 1.5 and 4.0 g in a fixed 50 mL reaction volume for a fixed 50:50 styrene/*n*-butyl acrylate comonomer mixture. (See entries 1−7 in Table 1.)

Silica incorporation efficiencies exceed 90% for initial silica sol concentrations up to 3.75 g, see Table 1. These values are comparable to those recently reported by Dupin and coworkers for non-film-forming nanocomposite particles prepared with a 2-vinylpyridine auxiliary comonomer.[22] It is also clear that a minimum amount of silica (3.0 g) is required to obtain stable nanocomposite particles under the chosen conditions. Weak flocculation of the nanocomposite particles is observed if the silica sol concentration is insufficient. For higher silica sol concentrations (above 3.75 g), there is evidence of a reduction in silica incorporation efficiency. Therefore there appears to be an optimum range of silica sol concentrations for this particular set of synthesis parameters.

Two methods were used to determine the silica incorporation efficiency. The first method involved measuring the mean silica content of nanocomposite particles after the removal of any excess silica sol by centrifugation. This silica content, together with the total comonomer conversion, allows calculation of the silica incorporation efficiency. The second method simply involved high-speed centrifugation of the reaction solution after the copolymerization to sediment the larger nanocomposite particles selectively. The concentration of the smaller excess silica sol remaining in the supernatant was then determined gravimetrically. In most cases, these two methods led to similar incorporation efficiencies, see Table 1. The first method is rather time-consuming, involves two separate measurements, each with its own source of experimental errors, and is more likely to underestimate the silica incorporation efficiency. In contrast, the second method is more convenient but assumes that the excess silica sol can be quantitatively separated from the nanocomposite particles. This may not be the case for smaller nanocomposite particles, and true silica incorporation efficiencies are likely to be overestimated in such cases. For both methods, there is also the possibility that silica particles that are only weakly adsorbed onto the surface of the nanocomposite particles may become detached during high-speed centrifugation.

Transmission electron micrographs of *unpurified* poly(styrene-*stat*-*n*-butyl acrylate)/silica nanocomposite dispersions prepared at 3.0 and 4.0 g initial silica sol (entries 3 and 7 in Table 1, respectively) are shown in Figure 2. There is evidence of partial particle coalescence on the TEM grid, which is not unexpected for the targeted low T_g copolymer compositions. In this context, it is perhaps worth emphasizing that DLS and DCP measurements confirmed that these film-forming nanocomposite particles had good colloid stability prior to TEM sample preparation. The TEM images shown in Figure 2 also confirm that some excess free silica is visible at higher initial silica sol concentrations. Purification, and therefore accurate characterization of the mean silica content, is nontrivial for these film-forming nanocomposite particles. One precaution involved centrifugation (at no more than 8000 rpm for 30 min, or 5018 g) using a precooled (5 °C) centrifuge chamber and rotor to avoid film formation of the sedimented nanocomposite particles. This careful centrifugation protocol enabled any excess silica sol to be removed, as judged by TEM. Particle densities of the purified nanocomposite particles varied from 1.34 to 1.41 g/cm^3, but there was no obvious correlation with the initial silica sol concentration, see Table 1. Mean silica contents ranged between 39 and 43 wt %; higher values were obtained at higher initial silica sol concentrations, but these differences are probably within experimental error. Therefore, these nanocomposite particles contain significantly more silica than the polystyrene/silica nanocomposite particles reported earlier.[19] There are two possible explanations. First, these new film-forming nanocomposite particles also have a "core−shell" morphology, and their silica contents are higher simply because of their smaller particle size. Alternatively, these new nanocomposite particles may exhibit a "raspberry" (framboidal) morphology, which is typically characterized by higher silica contents.[20]

Variation of the Styrene/*n*-Butyl Acrylate Mass Ratio. Further studies involved systematic variation of the styrene/*n*-butyl acrylate comonomer ratio, which inevitably affects the T_g of the resulting poly(styrene-*stat*-*n*-butyl acrylate)/silica nanocomposites and therefore also influences their minimum film-forming temperature. These results are summarized in Table 1, see entry 3 and entries 8 to 14. Unfortunately, only formulations comprising at least 50 wt % styrene resulted in the formation of colloidally stable nanocomposite particles under the stated conditions; acrylate-rich formulations invariably led to particle aggregation when using a fixed 3.0 g charge of silica sol. The colloidally stable nanocomposite particles had reasonably narrow particle size distributions, as judged by DLS and DCP measurements. TEM images are shown in Figure 2 and confirm a reduced propensity toward film formation for styrene-rich copolymers; individual nanocomposite particles can be observed for such formulations, and DCP data (Table 1) indicate larger mean particle diameters. Assuming that the "core−shell" morphology previously reported for polystyrene/silica nanocomposite particles is retained,[18,19] this trend in increasing particle size explains the monotonic increase in silica content and nanocomposite particle density observed for this series of copolymer/silica nanocomposites because of their increased surface area per unit mass. Indeed, the "core−shell" nature of these film-forming copolymer/silica nanocomposite particles is confirmed by ESI/TEM studies (see later).

Particle Growth and Monomer Conversion Study. The simultaneous evolution of particle growth and comonomer conversion with reaction time was elucidated using DLS and gravimetry for a 50:50 styrene/*n*-butyl acrylate formulation using an initial silica sol concentration of 3.0 g, see entry 3 in Table 1. This copolymerization was performed on a five-fold larger scale than the syntheses undertaken so far (i.e., 250 mL instead of 50 mL). This was necessary to minimize changes in component concentration due to the removal of successive aliquots. The results for this experiment are shown in Figure 3. As expected, there was a strong correlation between the final particle diameter and the comonomer conversion, with final values being attained within approximately 7.5 h.

Surface Characterization. The surface compositions of these nanocomposite particles were characterized by both aqueous electrophoresis and XPS. ζ potential versus pH curves for

Table 1. Effect of Varying the Synthesis Parameters on the Mean Density, Silica Content, Silica Aggregation Efficiency, and Particle Diameter of Poly(styrene-*stat*-*n*-butyl acrylate)/Silica Nanocomposite Particles Prepared by Aqueous Emulsion Copolymerization Using a Commercial 19 nm Bindzil CC40 Silica Sol and a Cationic AIBA Initiator[a]

entry no.	initial silica mass (g)	St/*n*-BuA mass ratio	comonomer conversion (%)[b]	particle density (g cm^{-3})[c]	silica content (wt %)[d]	silica incorporation efficiency from thermogravimetry (%)	silica incorporation efficiency from centrifugation (%)	number-average diameter by TEM (nm)	weight-average diameter by DCP (nm)	intensity-average diameter by DLS (nm)
1	1.5	50:50	flocculation							
2	2.0	50:50	flocculation							
3	3.0	50:50	97	1.34	39	100	100	154 ± 24	194 ± 46[e]	205 (0.041)
4	3.25	50:50	99	1.35	41	100	99	144 ± 15	174 ± 48	252 (0.129)
5	3.50	50:50	98	1.38	39	91	98	205 ± 22	181 ± 45	198 (0.033)
6	3.75	50:50	99	1.39	43	99	99	134 ± 16	151 ± 40	202 (0.069)
7	4.0	50:50	98	1.35	43	80	96	141 ± 19	147 ± 33	191 (0.036)
8	3.0	0:100	flocculation							
9	3.0	20:80	flocculation							
10	3.0	40:60	flocculation							
11	3.0	60:40	99	1.33	37	69	91	167 ± 19	163 ± 28	206 (0.016)
12	3.0	70:30	99	1.28	31	75	78	195 ± 27	186 ± 34	246 (0.099)
13	3.0	80:20	98	1.27	27	60	49	235 ± 26	204 ± 18	255 (0.036)
14	3.0	100:0	81	1.25	27	50	50	305 ± 25	281 ± 38	330 (0.060
15	none	50:50	97	1.05	n/a	n/a	n/a	619 ± 22	602 ± 80	667 (0.143)
16[f]	none	50:50	98	1.05	n/a	n/a	n/a			443 (0.038)
17[g]	none	50:50	97	1.05	n/a	n/a	n/a			240 (0.021)

[a] All copolymerizations were conducted using 5.0 g total comonomer in 50 mL of reaction volume and 50 mg AIBA at 60 °C for 24 h. [b] Determined gravimetrically. [c] Determined by helium pycnometry. [d] Determined by thermogravimetric analysis. [e] Close inspection of this DCP trace indicates a bimodal size distribution. [f] Cationic control copolymer latex prepared in the presence of 1.2 wt % (based on monomer) Triton X100 nonionic surfactant and cationic AIBA initiator. [g] Anionic copolymer latex prepared using an ammonium persulfate initiator in the presence of 0.30 wt % sodium dodecyl sulfate surfactant (based on monomer).

selected nanocomposite particles are shown in Figure 4. All poly(styrene-*stat*-*n*-butyl acrylate)/silica nanocomposites, whether prepared at a silica concentration of either 3.0 or 4.0 g (entries 3 and 7 in Table 1) or by varying the styrene/*n*-butyl acrylate mass ratio (from 50:50 for entry 3 to 70:30 for entry 12) at a fixed silica concentration, exhibit essentially the same electrophoretic behavior as the polystyrene/silica nanocomposite particles (entry 14) and the pristine silica sol (Bindzil CC 40). This suggests that the film-forming copolymer nanocomposite particles also exhibit a silica-rich particle surface, which is consistent with their postulated "core−shell" morphology.

With a typical sampling depth of 2−10 nm, XPS allows elemental analysis of the chemical composition of the nanocomposite surface.[21] Because film formation occurs upon drying at ambient temperature, subtle changes in nanocomposite surface morphology may occur, as reported by Percy et al. for poly(*n*-butyl acrylate-*stat*-4-vinylpyridine)/silica nanocomposite particles.[13] Thus the nanocomposite particles were carefully freeze-dried from aqueous solution to preserve their original particle morphology prior to XPS studies. The surface compositions of nanocomposite films cast from the 50:50 poly(styrene-*stat*-*n*-butyl acrylate)/silica particle dispersions at either room temperature or 70 °C were also examined by XPS. Table 2 summarizes the XPS results obtained for each of these samples, and the corresponding survey spectra for the poly(styrene-*stat*-*n*-butyl acrylate)/silica nanocomposite particles are provided in Figure S1 of the Supporting Information.

In all cases, the two silicon signals at 104 and 155 eV confirm the presence of the silica component at (or very near) the surface of the nanocomposite films or particles. More detailed information was obtained from the various silicon, carbon, and oxygen core-line spectra, which were used to determine the surface Si/C atomic ratios of the freeze-dried nanocomposite particles and the corresponding films. These XPS atomic ratios ranged from 0.23 to 0.30, see Table 2. These values should be compared with the bulk Si/C atomic ratio of 0.14 calculated from thermogravimetry. This indicates that both the nanocomposite films and particles have silica-rich surfaces, which is also consistent with the aqueous electrophoresis data. There is some evidence of film formation leading to a higher Si/C atomic ratio, which suggests silica enrichment at the film surface. However, this increase is not particularly large and is comparable to the overall experimental error. Nevertheless, these XPS observations are in contrast with those reported by Percy et al., who observed copolymer enrichment at the hydrophobic air/film interface.[17] Silica enrichment of the nanocomposite film surface is desirable for applications in paints and coatings because this leads to a tougher, more durable coating that is potentially both dirt-shedding and scratch-resistant.[5]

In addition, the observation of a distinct carbonyl component in the C1s core-line spectra (Figure S2 in Supporting Information) confirms the presence of the *n*-butyl acrylate comonomer at the surface of the 50:50 poly(styrene-*stat*-*n*-butyl acrylate)/silica nanocomposite film. This is consistent with this comonomer interacting with either the silanol or glycerol groups on the surface of the silica nanoparticles. Glass transition temperatures (T_g) were determined for four poly(styrene-*stat*-*n*-butyl acrylate)/silica nanocomposites as well as a polystyrene/silica nanocomposite using differential scanning calorimetry. These data were compared with the theoretical T_g values calculated using the well-known Fox equation, which assumes no specific interactions between comonomers. These results are summarized in Table 3. The difference between these two data sets (ΔT_g) becomes more pronounced as the proportion of acrylate comonomer in the copolymer/silica nanocomposite particles is increased, with little or no discrepancy being observed for the polystyrene/silica nanocomposite. Taken together with the XPS observations, this suggests that there are indeed specific interaction(s) between the inorganic silica particles and the acrylic comonomer units in the copolymer chains. One obvious possibility would be a hydrogen bonding-type interaction between the surface glycerol and/or silanol groups on the silica and the ester carbonyl groups of the *n*-butyl acrylate. Solid-state NMR studies are now in progress to assess the precise nature to further assess this molecular interaction.

Electrospray Ionization/Transmission Electron Microscopy Studies. We have previously reported that ESI/TEM is a powerful technique for assessing the morphology of vinyl polymer/silica nanocomposite particles.[20] The film-forming 50:50 poly(styrene-*stat*-*n*-butyl acrylate)/silica nanocomposite particles (sample 3 in Table 1) were examined using ESI/TEM in combination with ultramicrotomy. In the bright-field image of Figure 5, the cross-sectioned particles are clearly surrounded

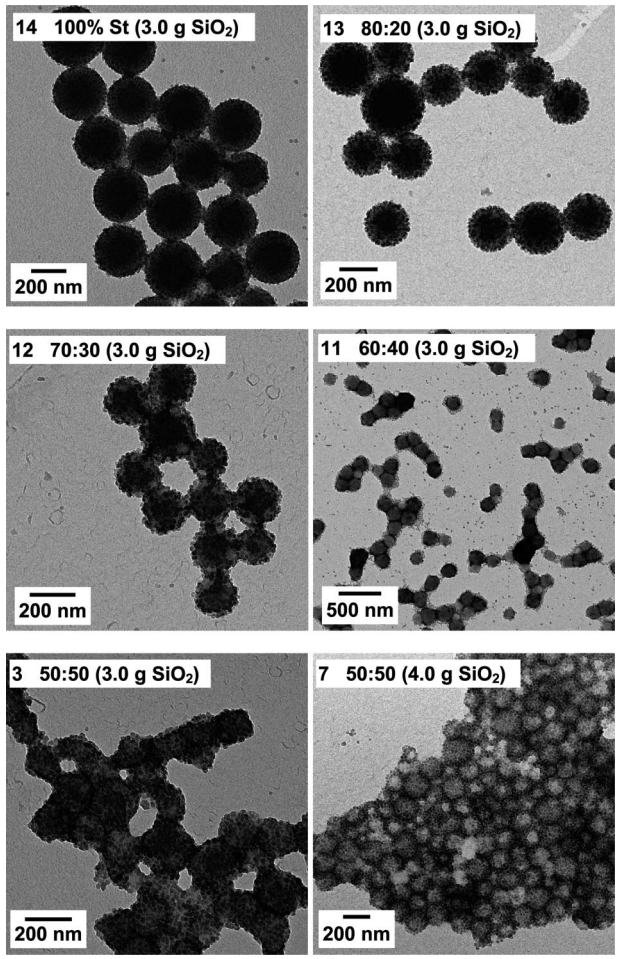

Figure 2. TEM images of nanocomposite particles prepared by emulsion copolymerization using various styrene/*n*-butyl acrylate mass ratios in the presence of a glycerol-modified silica sol (Bindzil CC40). Polymerizations were conducted using 3.0 g silica sol, 5.0 g total comonomer (for example, 2.5 g styrene and 2.5 g *n*-butyl acrylate for the two 50:50 formulations), and 50.0 mg cationic AIBA initiator at 60 °C for 24 h. Increasing particle coalescence can be observed with increasing *n*-butyl acrylate content. Dynamic light scattering experiments (not shown) confirm that no particle aggregation occurred prior to drying.

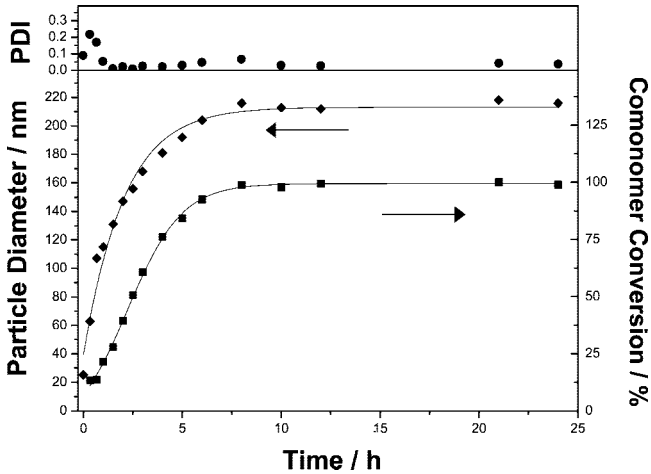

Figure 3. Evolution of mean particle diameter, polydispersity index, and comonomer conversion for a nanocomposite synthesis conducted at a 50:50 styrene:*n*-butyl acrylate mass ratio by emulsion copolymerization with cationic AIBA initiator at 60 °C for 24 h (see entry 3 in Table 1; this synthesis was scaled up five-fold).

by a honeycomb-like structure of silica particles. The carbon and silicon elemental maps confirm that each nanocomposite particle consists of a carbon-rich copolymer core surrounded by a thin shell of silica sol. Therefore these poly(styrene-*stat*-*n*-butyl acrylate)/silica nanocomposite particles have a well-defined "core−shell" particle morphology.

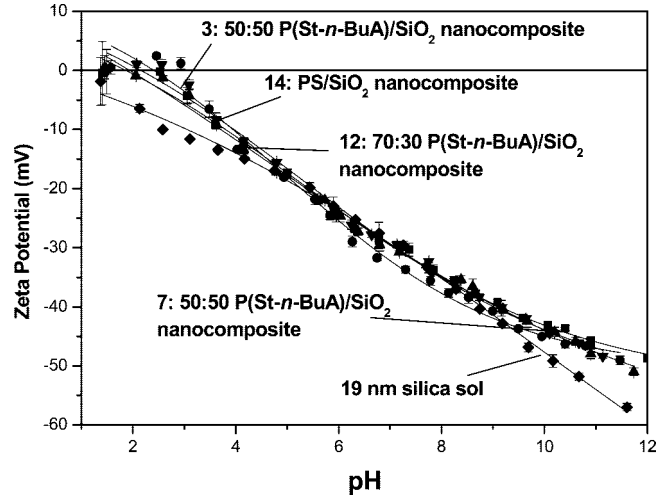

Figure 4. Aqueous electrophoresis curves obtained for various nanocomposite particles: 50:50 and 70:30 styrene/*n*-butyl acrylate mass ratios prepared using 3.0 g Bindzil CC40 silica sol (entries 3 and 12 in Table 1, respectively), a 50:50 styrene/*n*-butyl acrylate nanocomposite prepared using 4.0 g initial silica sol (entry 7 in Table 1), a polystyrene/silica nanocomposite (entry 14 in Table 1), and the corresponding pristine Bindzil CC40 silica sol. The total (co)monomer amount was 5.0 g, the AIBA initiator was fixed at 50 mg, and all (co)polymerizations were conducted 60 °C for 24 h.

Table 2. Summary of Surface Atomic Percentages for Carbon, Oxygen, and Silicon Obtained from XPS Core-Line Spectra Recorded for Poly(styrene-*stat*-*n*-butyl acrylate)/Silica Nanocomposites Prepared Using a 50:50 Styrene/*n*-Butyl Acrylate Comonomer Mass Ratio[a]

sample description	St/*n*-BuA mass ratio	C1s atom %	O1s atom %	Si2p atom %	Si/C atomic ratio by XPS[b]
nanocomposite particles	50:50	60.5	25.3	14.2	0.23
nanocomposite film, 20 °C	50:50	57.1	26.7	16.1	0.28
nanocomposite film, 70 °C	50:50	54.8	28.9	16.3	0.30
nanocomposite film, after combustion	50:50	11.1	55.2	33.8	3.05
P(St-*n*-BuA) latex (control)	50:50	87.9	11.2	0.9	0.01

[a] Surface composition of the freeze-dried nanocomposite particles (no film formation) was compared with that of the corresponding nanocomposite films prepared at either 20 or at 70°C. Data obtained for the residual black monolithic char formed after combustion of a nanocomposite film and a copolymer latex control are also shown. [b] XPS Si/C atomic ratios were determined from individual core-line spectra.

Table 3. Comparison of Theoretical and Experimental Glass Transition Temperatures (T_g) Obtained for a Series of Poly(styrene-*n*-butyl acrylate)/Silica Nanocomposite Particles Prepared Using Various Styrene/*n*-Butyl Acrylate Mass Ratios

St/*n*-BuA mass ratio	theoretical T_g (°C)[a]	onset T_g by DSC (°C)[b]	ΔT_g (°C)
50:50	4.3	19.3	15.0
60:40	19.9	33.1	13.2
70:30	37.4	45.1	7.7
80:20	57.1	63.6	6.5
100:0	105.0	107.5	2.5

[a] As calculated from the Fox equation using homopolymer T_g values of 105 °C for polystyrene and −54 °C for poly(*n*-butyl acrylate). [b] Differential scanning calorimetry.

Film Transparency. The optical transparency of various nanocomposite films was assessed. Therefore, differing volumes of an aqueous dispersion of a 50:50 poly(styrene-*stat*-*n*-butyl

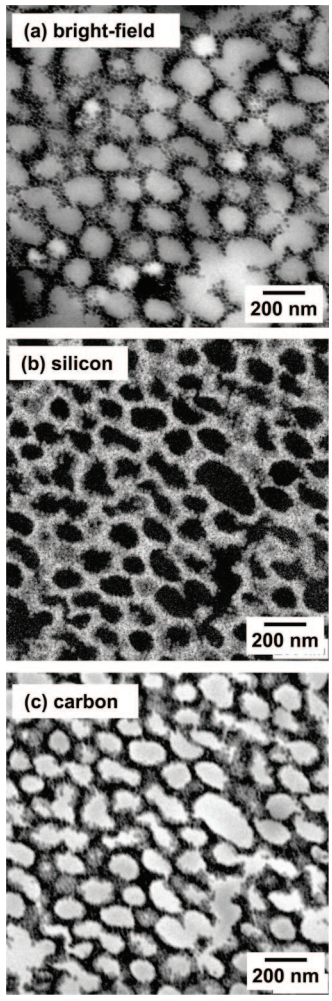

Figure 5. TEM images of ultramicrotomed poly(styrene-*stat*-*n*-butyl acrylate)/silica nanocomposite particles (entry 3 in Table 1). (a) The bright-field image and the two elemental maps obtained for (b) silicon and (c) carbon reveal that these film-forming nanocomposite particles possess a distinct "core−shell" morphology, whereby the copolymer component forms the core, and the silica particles form the shell. This particular nanocomposite was prepared using 50:50 styrene/*n*-butyl acrylate; samples prepared using other mass ratios exhibited similar core−shell morphologies (data not shown).

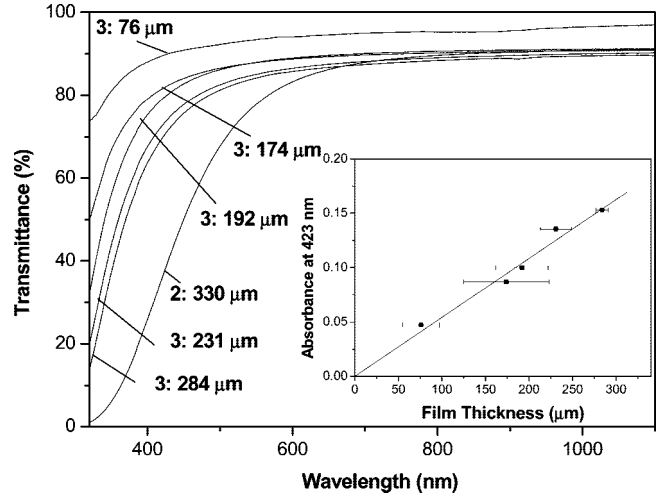

Figure 6. Transmission mode visible absorption spectra recorded for poly(styrene-*stat*-*n*-butyl acrylate)/silica nanocomposite films prepared from sample 3 (Table 1) with various thicknesses. A comparative film prepared from sample 2 (Table 1), which was appreciably flocculated prior to film formation, led to substantially reduced transparency. The inset shows a linear relationship between absorbance (λ = 423 nm) and film thickness and thus confirms the expected Beer−Lambert law.

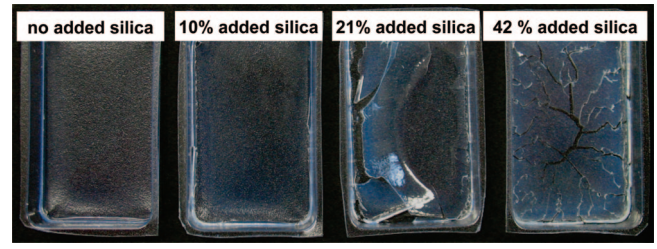

Figure 7. Digital photographs of 50:50 poly(styrene-*stat*-*n*-butyl acrylate)/silica nanocomposite films (mean thickness 200 ± 41 μm; entry 3 in Table 1) that were deliberately contaminated with varying amounts of glycerol-functionalized silica sol (Bindzil CC40). Addition of this excess silica sol leads to significant film embrittlement upon drying. This illustrates the importance of achieving high silica aggregation efficiencies in these colloidal nanocomposite syntheses. Images were recorded with the films still in their plastic molds because they were too brittle to remove intact.

acrylate)/silica nanocomposite (entry 3 in Table 1) were dried in plastic molds at room temperature, leading to free-standing nanocomposite films of varying thickness. After determining the mean thickness of each film using a micrometer screw gauge, film transmittances were assessed using visible absorption spectroscopy, see Figure 6. Alternatively, if the film transparency is expressed in terms of absorbance rather than transmittance, then it can be shown that the Beer−Lambert law is valid for these nanocomposite films, see inset shown in Figure 6.

For film thicknesses ranging from 76 to 284 μm, the transmission exceeded 80% above a wavelength of 500 nm. Given that these films contain 38 wt % of silica, these observations strongly suggest that the silica nanoparticles must be homogeneously dispersed within the film, with domain sizes substantially smaller than the wavelength of visible light. The films were less transparent at shorter wavelengths, but even the thickest film still had a transmittance of more than 50% above 371 nm. For comparative purposes, a film cast from flocculated nanocomposite particles (prepared using a formulation with a relatively low silica sol concentration; entry 2 in Table 1) was also examined. This film was visibly opaque (Figure S3 in the Supporting Information) and exhibited a transmittance of only 25% at 400 nm. The Beer−Lambert law can be used to correct for the difference in film thickness between this opaque film and the transparent 284 μm nanocomposite film (whose visible absorption spectrum is also shown in Figure 6). This analysis leads to film transmittances (at 423 nm) of only 40% for the flocculated nanocomposite particles (entry 2, Table 1) but more than 70% for the colloidally stable nanocomposite particles (entry 3, Table 1). This observation confirms the importance of colloidal stability for the preparation of high-quality transparent nanocomposite films.

To systematically study the effect of excess silica sol on film formation, we deliberately contaminated a nanocomposite sample (entry 3 in Table 1) by adding various amounts of the Bindzil CC40 silica sol. Here the percentage of excess silica was calculated on the basis of the amount of silica present in the original nanocomposite film (38% by mass). This controlled addition of excess silica sol still led to fairly transparent nanocomposite films, see Figure 7 and also Figure S4 in the Supporting Information. However, substantial film cracking was observed above 21% added silica (i.e., 46% total silica content). In summary, these negative results confirm that high silica aggregation efficiencies are highly desirable for the synthesis of high-quality vinyl polymer/silica nanocomposite films.

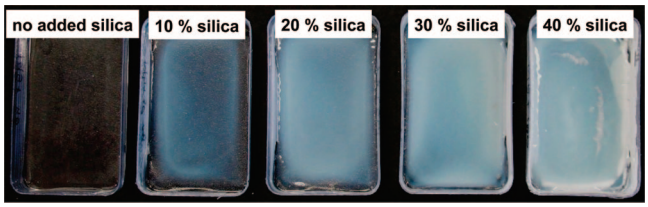

Figure 8. Digital photographs of nanocomposite films (mean film thickness 302 ± 53 μm) prepared from admixtures of a cationic poly(styrene-*stat*-*n*-butyl acrylate) copolymer latex (prepared using a 50:50 styrene/*n*-butyl acrylate mass ratio) with varying amounts of glycerol-functionalized silica sol (Bindzil CC40). Addition of this excess silica sol led to opaque films. This suggests that the in situ copolymerization route to colloidal nanocomposites confers a genuine advantage over simple admixtures of latexes and silica sols. Images were recorded with the films still in their plastic molds because they were too brittle to remove intact.

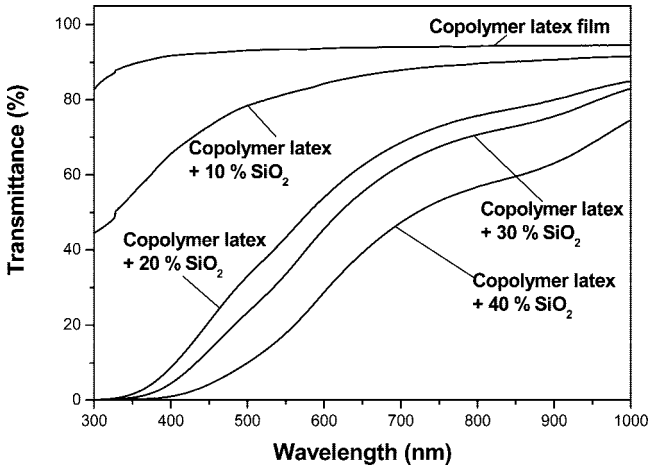

Figure 9. Transmittance measurements recorded by visible absorption spectroscopy for free-standing cationic poly(styrene-*stat*-*n*-butyl acrylate) copolymer latex films (50:50 styrene/*n*-butyl acrylate mass ratio) prepared in the presence and absence of varying amounts of deliberately added silica sol. Even at an excess silica content of only 10%, significantly reduced transparency is observed for the latex/silica composite film.

Nanocomposite Control Films. In principle, nanocomposite films can be prepared by simply mixing a silica sol with a film-forming latex,[23] and thus it is important to consider whether the in situ copolymerization approach described in the present study confers any useful performance benefit. Therefore, two sets of control experiments were performed in which film-forming 50:50 poly(styrene-*stat*-*n*-butyl acrylate) copolymer latexes were mixed with various amounts of the glycerol-functionalized silica sol. First, cationic copolymer latex (entry 16 in Table 1) was prepared by copolymerizing styrene and *n*-butyl acrylate using the AIBA initiator in the presence of a nonionic surfactant (Triton X100). This cationic copolymer latex was expected to exhibit an electrostatic interaction with the anionic silica sol, similar to that proposed during the nanocomposite particle formation.[18,19] Indeed, upon mixing various amounts of silica sol with this latex, an immediate increase in viscosity was observed for the aqueous dispersions, which became somewhat flocculated. As expected, latex/silica films prepared from such dispersions exhibited only very limited transparency, as judged by both visual inspection (Figure 8) and transmittance measurements (Figure 9). This suggests that there is significant aggregation of the relatively high refractive index silica nanoparticles within these latex/silica films, which causes extensive light scattering. Second, anionic copolymer latex (entry 17 in Table 1) was prepared using a persulfate initiator combined with an anionic surfactant (sodium *n*-dodecyl sulfate). This latex formulation was selected to ensure that there was no electrostatic interaction with the silica sol. The addition of varying amounts of silica sol to this anionic copolymer latex did not lead to any increase in viscosity or loss in colloidal stability. However, only relatively opaque latex/silica films could be cast from aqueous solution, even when their silica sol content was as low as 10 wt %, see Figures S5 and S6 in the Supporting Information. Hence these control experiments suggest that in situ (co)polymerization offers a potentially decisive advantage over simple admixtures of preformed copolymer latex and silica sol for the preparation of high-quality transparent nanocomposite films.

Burning Behavior. It is widely recognized that polymer-inorganic oxide nanocomposites often exhibit enhanced fire retardancy during combustion.[24−27] In general, a reduction in peak heat release rate of the nanocomposite is observed relative to the corresponding pristine (co)polymer. However, this is not a prerequisite. For example, Calvert and coworkers[25] investigated the flammability behavior of nylon-6/layered silicate nanocomposites. Although no change in peak decomposition temperature was detected in this case, no molten plastic droplets were observed during combustion at a clay content of 10 wt %. Such droplets allow fires to spread rapidly, and hence their elimination is considered to be highly desirable.

To investigate whether similar improvements could be achieved for the nanocomposite materials prepared in the present study, a simple qualitative test was performed. The combustion of a 50:50 poly(styrene-*stat*-*n*-butyl acrylate)/silica nanocomposite film (sample 3 in Table 1) was compared with that of a film cast from a 50:50 poly(styrene-stat-*n*-butyl acrylate) latex prepared in the absence of any silica (sample 15 in Table 1). Digital images of the latter copolymer latex film recorded at different time intervals after ignition are shown in Figure 10. This copolymer latex film burnt completely with the formation of multiple molten plastic droplets. Such behavior constitutes a major fire hazard. The nanocomposite film also ignites readily. However, its combustion is much more controlled, with no molten droplets being observed. After the organic component has been consumed, the predominately silica framework remains as a black monolithic char. XPS analysis of this silica-rich char indicated a surface carbon content of 11 atom % and a Si/C atomic ratio of 3.05, see Table 2. Such burning behavior is much more desirable compared with that observed for the corresponding copolymer latex film and therefore represents a significant improvement in fire retardant behavior.

Conclusions

Copolymerizing *n*-butyl acrylate with styrene in the presence of a commercial glycerol-functionalized aqueous silica sol leads to the formation of film-forming colloidal nanocomposite particles with mean particle diameters of 147 to 235 nm and silica contents ranging from 27 to 43 wt %. Optimization of the initial silica sol concentration used in such syntheses allows silica incorporation efficiencies of almost 100% to be achieved. Particle growth curves confirmed that the nanocomposite particles attain their final diameter within 7.5 h, which corresponds to a comonomer conversion of more than 98%. Varying the styrene/*n*-butyl acrylate mass ratio under the stated conditions only produced colloidally stable nanocomposite particles if styrene comprised at least 50% of the comonomer feed by mass. Increasing the styrene content in the comonomer feed above 50% led to a systematic increase in mean particle diameter and a concomitant reduction in silica incorporation efficiency. Drying aqueous nanocomposite dispersions prepared at a 50:50 styrene/*n*-butyl acrylate mass ratio at room temperature results in highly transparent films. The transparency of such films (containing 38 wt % silica) decreases with increasing film

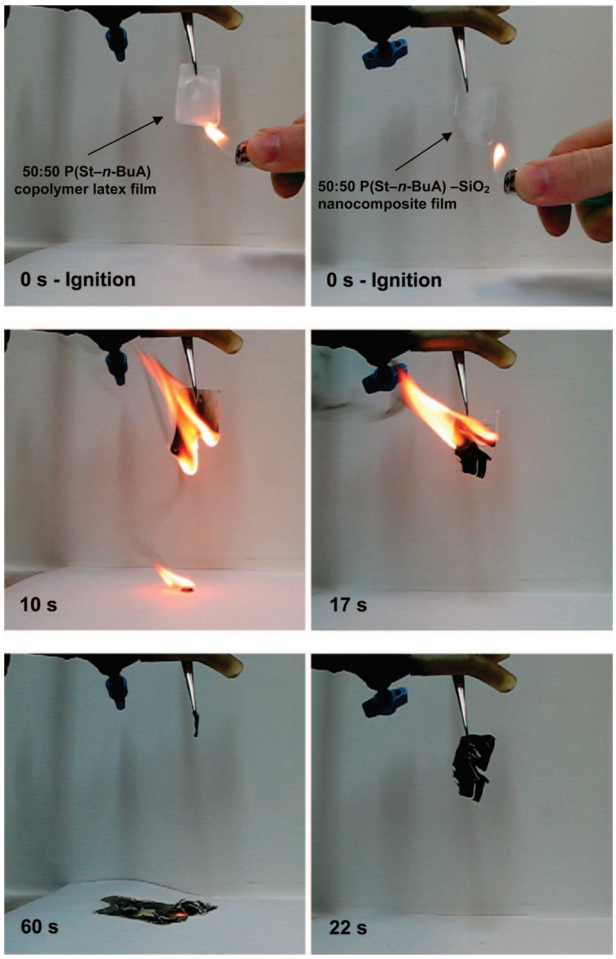

Figure 10. Digital photographs of the burning behavior of a 50:50 poly(styrene-*stat*-*n*-butyl acrylate) copolymer latex film (left-hand set of images) recorded at different times. Combustion is accompanied by substantial dripping of molten latex droplets, which is a major fire hazard. In contrast, a 50:50 poly(styrene-*stat*-*n*-butyl acrylate)/silica nanocomposite film (right-hand set of images) burns without dripping to form a black monolithic char. Such burning behavior is considered to be much less hazardous.

thickness, as judged by visible absorption spectroscopy. Markedly less transparent films that were much more prone to cracking were obtained if the dispersion was deliberately contaminated with excess silica sol prior to film formation. This highlights the need for high silica aggregation efficiencies in such nanocomposite syntheses. Composite films prepared by simply mixing silica sol with a preformed film-forming copolymer latex led to significantly less transparent films, even at relatively low silica contents. This illustrates the utility of the in situ (co)polymerization approach for the synthesis of colloidal nanocomposite particles. During film formation at either room temperature or elevated temperature, the surface of the nanocomposite film becomes slightly enriched in silica, as judged by XPS. Combustion of a nanocomposite film produced a monolithic char, whereas combustion of a corresponding copolymer latex film proved to be far more hazardous. Therefore these nanocomposite films exhibit promising fire-retardant behavior.

Acknowledgment. We thank The University of Sheffield for a Ph.D. studentship for AS. SPA is the recipient of a five-year Royal Society Wolfson Trust Research Merit Award. We thank Dr. Peter Greenwood of Eka Chemicals (Bohus, Sweden) for donating the Bindzil CC40 and CC30 aqueous silica sols.

Supporting Information Available: XPS survey and core-line spectra of freeze-dried nanocomposite powder and films, digital photographs, and visible absorption spectra of nanocomposite films prepared in various control experiments. This material is available free of charge via the Internet at http://pubs.acs.org.

References and Notes

(1) Bourgeat-Lami, E. *J. Nanosci. Nanotechnol.* **2002**, *2*, 1.
(2) Balmer, J. A.; Schmid, A.; Armes, S. P. *J. Mater. Chem.* **2008**, *18*, 5722.
(3) Wang, T.; Keddie, J. L. *Adv. Colloid Interface Sci.* **2009**, *147−148*, 319.
(4) Zou, H.; Wu, S.; Shen, J. *Chem. Rev.* **2008**, *108*, 3893.
(5) (a) Leuninger, J.; Tiarks, F.; Wiese, H.; Schuler, B. *Farbe + Lack* **2004**, *110*, 30. (b) Xue, Z.; Wiese, H. *U.S. Patent no. 7,094,830*, **2006**;(c) Tiarks, F.; Leuninger, J.; Wagner, O.; Jahns, E.; Wiese, H. *Surf. Coat. Int.* **2007**, *5*, 221.
(6) Fujii, S.; Armes, S. P. *Adv. Mater.* **2005**, *17*, 1014.
(7) Fujii, S.; Armes, S. P.; Binks, B. P.; Murakami, R. *Langmuir* **2006**, *22*, 6818.
(8) Goldsworthy, B. J.; Burchell, M. J.; Cole, M. J.; Green, S. F.; Leese, M. R.; McBride, N.; McDonnell, J. A. M.; Müller, M.; Grün, E.; Srama, R.; Armes, S. P.; Khan, M. A. *Adv. Space Res.* **2002**, *29*, 1139.
(9) Barthet, C.; Hickey, A. J.; Cairns, D. B.; Armes, S. P. *Adv. Mater.* **1999**, *11*, 408.
(10) Percy, M. J.; Barthet, C.; Lobb, J. C.; Khan, M. A.; Lascelles, S. F.; Vamvakaki, M.; Armes, S. P. *Langmuir* **2000**, *16*, 6913.
(11) Percy, M. J.; Amalvy, J. I.; Randall, D. P.; Armes, S. P.; Greaves, S. J.; Watts, J. F. *Langmuir* **2004**, *20*, 2184.
(12) Percy, M. J.; Michailidou, V.; Armes, S. P.; Perruchot, C.; Watts, J. F.; Greaves, S. J. *Langmuir* **2003**, *19*, 2072.
(13) Amalvy, J. I.; Percy, M. J.; Armes, S. P.; Wiese, H. *Langmuir* **2001**, *17*, 4770.
(14) Tiarks, F.; Landfester, K.; Antonietti, M. *Langmuir* **2001**, *17*, 5775.
(15) Zhou, J.; Zhang, S.; Qiao, X.; Li, X.; Wu, L. *J. Polym. Sci., Part A: Polym. Chem.* **2006**, *44*, 3202.
(16) Qi, D.-M.; Bao, Y.-Z.; Weng, Z.-X.; Huang, Z.-M. *Polymer* **2006**, *47*, 4622.
(17) Schmid, A.; Fujii, S.; Armes, S. P.; Leite, C. A. P.; Galembeck, F.; Minami, H.; Saito, N.; Okubo, M. *Chem. Mater.* **2007**, *19*, 2435.
(18) Schmid, A.; Tonnar, J.; Armes, S. P. *Adv. Mater.* **2008**, *20*, 3331.
(19) Schmid, A.; Armes, S. P.; Leite, C. A. P.; Galembeck, F. *Langmuir* **2009**, *25*, 2485.
(20) Amalvy, J. I.; Percy, M. J.; Armes, S. P.; Leite, C. A. P.; Galembeck, F. *Langmuir* **2005**, *21*, 1175.
(21) Percy, M. J.; Amalvy, J. I.; Barthet, C.; Armes, S. P.; Greaves, S. J.; Watts, J. F.; Wiese, H. *J. Mater. Chem.* **2002**, *12*, 697.
(22) Dupin, D.; Schmid, A.; Balmer, J. A.; Armes, S. P. *Langmuir* **2007**, *23*, 11812.
(23) Balmer, J. A.; Armes, S. P.; Fowler, P. W.; Tarnai, T.; Gáspár, Z.; Murray, K. A.; Williams, N. S. J. *Langmuir*, in press.
(24) Yang, F.; Yngard, R.; Nelson, G. L. *J. Fire Sci.* **2005**, *23*, 209.
(25) Shanumuganathan, K.; Deodhar, S.; Dembsey, N.; Fan, Q.; Calvert, P. D.; Warner, S. B.; Patra, P. K. *J. Appl. Polym. Sci.* **2007**, *104*, 1540.
(26) Zhu, J.; Morgan, A. B.; Lamelas, F. J.; Wilkie, C. A. *Chem. Mater.* **2001**, *13*, 3774.
(27) Gilman, J. W.; Jackson, C. L.; Morgan, A. B.; Harris, R.; Manias, E.; Giannelis, E. P.; Wuthenow, M.; Hilton, D.; Phillips, S. H. *Chem. Mater.* **2000**, *12*, 1866.

MA900465K